Pulse Combustor Modeling Demonstration of the Importance of Characteristic Times

P. K. BARR, J. O. KELLER, and T. T. BRAMLETTE

Combustion Research Facility, Sandia National Laboratories, Livermore, CA 94551

C. K. WESTBROOK

Lawrence Livermore National Laboratory, University of California, Livermore, CA 94550

and

J. E. DEC*

University of Michigan, Ann Arbor, MI 48109

A numerical model has been developed to study the sensitivity of a pulse combustor's performance to changes in the relative timing between several of the dominant physical processes. The model is used to demonstrate the importance of the characteristic times associated with acoustics, fluid mixing, and chemical kinetics, which have been identified from both theoretical and experimental evidence. The combination of submodels for acoustics, injection, and combustion produces a pulse combustor model that is dynamic in that it fully couples the injection and mixing processes to the acoustic waves. Comparisons of simulations with experimental results show good agreement, verifying the model over a wide range of operating conditions. Because the model provides more control of the dominant processes than can be obtained in experiments, the parametric study establishes the cause-effect relation between the characteristic times and the resulting combustor performance.

INTRODUCTION

The underlying physical phenomenon controlling the dynamics of pulse combustion was explained before the turn of the century by Rayleigh [1]. Although much time has passed since then, a fundamental understanding of pulse combustor operation does not exist because the strong interactions among the dominant processes are highly coupled. They involve a multidimensional, transient flow field that is highly turbulent, with variable transport properties, a resonant acoustic pressure field, and a large transient energy release whose characteristic time is on the same order as the characteristic time for the fluid dynamics.

In general, pulse combustors use a periodic combustion process to drive a resonant pressure wave. The design under consideration here is known as a Helmholtz-type pulse combustor, shown in Fig. 1. It consists of a closed cylinder, which acts as the combustion chamber, that is

* Current address: Sandia National Laboratories, Livermore, CA 94551.

0010-2180/90/$3.50

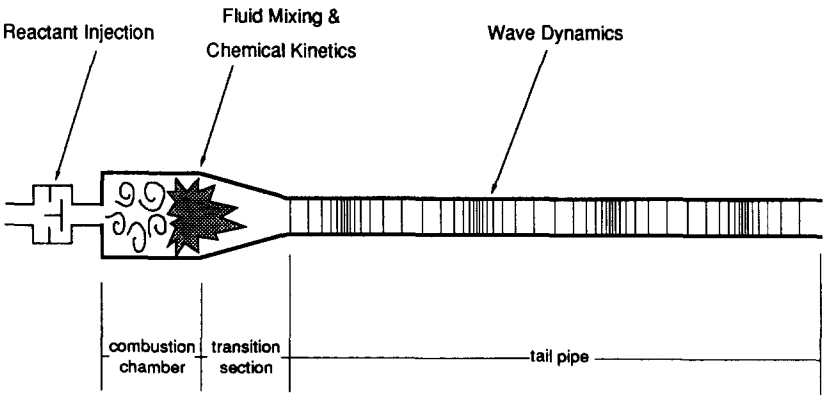

Fig. 1. Schematic of a Helmholtz-type pulse combustor, showing dominant processes that are combined in the model.

attached to a long tail pipe through a transition section. Injection of reactants is controlled by a one-way valve (either a flapper or an aerodynamic valve). Combustion of the reactants in the combustion chamber causes the pressure to rise and sends a compression wave down the tail pipe. This compression wave reflects off the exit of the tail pipe as an expansion wave. When this wave reaches the combustion chamber, it is reflected off the valved end as another expansion wave, causing the pressure in this chamber to drop below the reactant supply pressure. When the expansion wave reaches the tail pipe exit, it is reflected off the open end as a compression wave. The low pressure in the combustion chamber pulls reactants through the valve. The cold reactants mix with the hot products from previous cycles, and reignition occurs. In order for the combustion to reinforce the pressure oscillation, the reignition and combustion need to be in phase with the compression wave as it returns to the combustion chamber, because both the compression wave and the combustion act to raise the pressure. The increase in pressure stops the flow of reactants and again sends a compression wave down the tail pipe, and the cycle repeats.

Although a significant amount of research has been performed on pulse combustors, most of this work has been directed toward examining the overall characteristics of pulse combustors rather than understanding the fundamental controlling physics [2–4]. Because of the lack of fundamental information, the design and development of pulse combustors has proceeded largely by trial and error (or, appropriately, "cut-and-try"), a method that is time consuming, costly, and that does not guarantee an optimum design. An excellent discussion of design recommendations for pulse combustion burners is given by Vishwanath [5], in a report that is based on data obtained over several years from many different pulse combustor configurations.

Various theoretical models have been developed to simulate the performance of pulse combustors [6–12]. However, the degree of complexity of the processes that occur within a pulse combustor has required that these models use empirical relationships and/or experimentally determined information. Because this information is dependent on the pulse combustor configuration, a truly predictive capability does not yet exist. The coupling between controlling mechanisms must be understood before a predictive model can be developed.

The importance of the phase relation between the combustion chamber pressure and the cyclic energy release, first discussed by Rayleigh in 1878 [1], was demonstrated experimentally in a Helmholtz-type pulse combustor by Keller et al. [13, 14] and numerically shown by Barr et al. [12]. Although their one-dimensional numerical model simulated the wave motion throughout the entire pulse combustor, it required experimentally determined time-varying energy release and gas injection data. In another simulation study, Tsujimoto and Machii [15] used the method of characteristics to study the effect of the time lag between

the injection and combustion on pulsation stability. Assumed injection and energy release profiles were used in their investigation of the effects of injection timing, again verifying Rayleigh's criterion.

The work described in this article combines the one-dimensional wave model used by Barr et al. [12] with submodels to describe both the fuel–air injection and the energy release processes. The submodels allow both the injection and the combustion to depend on the cyclic-varying conditions in the combustion chamber. Each of these submodels has a single constant that is adjusted to the specific injection geometry and reactant mixture, thus minimizing the dependence on experimental data. Experimental data are used to fix the constants for one case; the submodels then predict the trends for other cases. This article demonstrates that the combination of these submodels can be used to simulate the stable operation and to determine the operational envelop of a Helmholtz-type pulse combustor. Additional simulations show the significance of changes to different time scales that are of importance to the overall operation of a pulse combustor.

RAYLEIGH'S CRITERION AND CHARACTERISTIC TIMES

In 1878, Rayleigh identified a fundamental requirement for stable combustion-drive pressure oscillations [1]. He pointed out that for the combustion process to drive pressure waves, the energy release must be in phase with the pressure cycle. Although the injection of both the fuel and air is controlled by the low-pressure portion of the cycle, different mechanisms control the timing of the high-pressure wave and the combustion of the gas. The temperature distribution within the entire combustor affects the wave propagation speed, and so determines the time required for waves to propagate the length of the combustor. This controls the time-varying pressure in the combustion chamber. The characteristic resonance time is called τ_{acoustic}. The cold reactant will not burn until several things have occurred. First, the fuel and air must mix to a concentration that can burn. This mixing process is controlled in part by the fluid mechanics of the injection process. Fluid mechanics also controls the rate at which the cold combustible gas mixes with the hot products, heating it to a temperature at which it can react. Finally, a finite amount of time is then required for the hot reactants to undergo combustion. These time scales are referred to as τ_{species} for the time required for the fuel and air to mix to a combustible ratio, τ_{mixing} for the time required for the combustible reactants to mix with the hot products to a temperature at which reaction can occur, and τ_{kinetic} for the time required for the chemical reaction to take place.

Rayleigh's criterion states that the maximum pulsation strength will occur when the pressure wave and the energy release profile are entirely in phase with each other. Several papers [13–17] have reported the effect of variations of the energy release to the overall operation of a pulse combustor. Because the pulsation strength and stability are sensitive to the relative timing of the pressure wave and the energy release profile, the pulse combustor operation can be adjusted by tuning the energy release profile to the acoustic wave.

In the work presented in this article the pulse combustor operation has been simplified by premixing the fuel and air before it is injected into the combustion chamber. This eliminates one of the time scales, τ_{species}, from the problem. The premixing is also advantageous because experimental results have shown that the combustor runs more stably and controllably by premixing the gases [13, 14].

This article presents results that show the effectiveness of tuning the energy release to the acoustic wave. Following the description of the model, it is verified by comparing the results from several sets of simulations with experimental data. The effects of the time scales τ_{acoustic}, τ_{mixing}, and τ_{kinetic} are studied, and the results of the pulse combustor performance are described in terms of these characteristic times.

THE NUMERICAL MODEL

The computational algorithm couples the wave dynamics to the combustion process by allowing each to affect the other until both obtain a repeatable solution. In addition to a submodel that

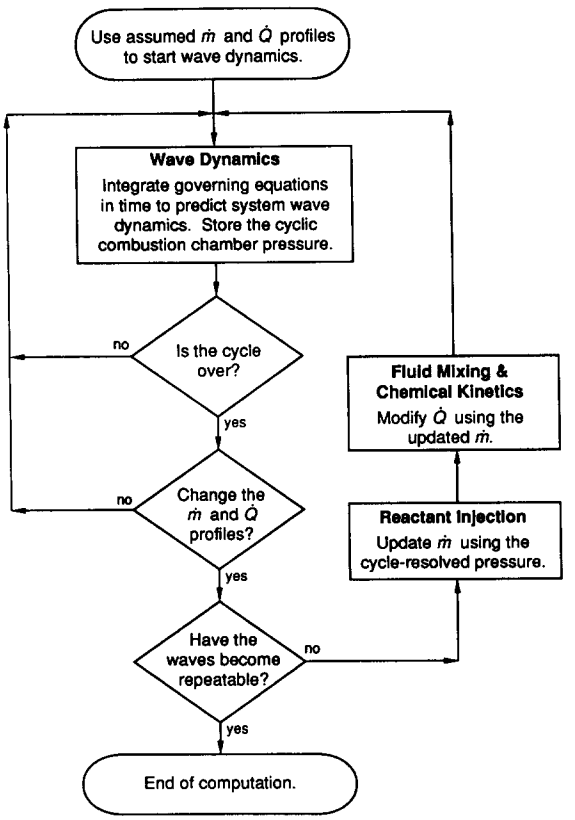

Fig. 2. Flowchart showing how the submodels are coupled in the model. Submodels are indicated by boldface type.

determines the wave dynamics, the model combines submodels for injection, mixing and chemical kinetics to determine the periodic combustion process that drives the wave dynamics. Because the reactant injection depends on the cycle-varying pressure in the combustion chamber, the submodels are coupled. This coupling is indicated on the flowchart presented in Fig. 2, where the boldface type indicates the four submodels in the pulse combustor model. Each of these submodels is described separately in this section.

The numerical algorithm is as follows. Because the dynamic pulse combustor model requires an existing pressure wave to drive the flow through the flapper valve, the simulation is started in a forced mode. That is, the injection and energy release profiles $\dot{m}$ and $\dot{Q}$ are prespecified, and they are repeatedly imposed on the initially cool system for several cycles at a fixed frequency. The initial $\dot{m}$ and $\dot{Q}$ profiles were selected to give a reasonable representation of the shapes observed in operating pulse combustors, although the final solution is not sensitive to the actual shape of these assumed profiles (provided that, when the dynamic submodels are activated, the pressure oscillations in the combustion chamber are strong enough to pull mass through the flapper valve).

After the model has been running in the forced mode long enough to set up pressure waves (30 cycles for the simulations presented here), it is switched to the dynamic mode. In this mode, the injection and energy release are coupled to the combustion chamber pressure, which is used to determine the operating frequency. Because the pressure is strongly dependent on the $\dot{m}$ and $\dot{Q}$ profiles, the entire system must converge to a compatible solution in order to maintain stable, repeatable pulsations. The time history of the pressure in the combustion chamber is recorded over one cycle, where a single cycle is now defined by the downward-going zero crossing of the combustion chamber pressure (relative to atmospheric pressure). The time between these two pressure points determines the operating frequency. The injection submodel uses the recorded pressure signal to determine the time-varying flow rate $\dot{m}$ through the flapper valve. The mass injection profile $\dot{m}$ is used by the mixing and kinetics submodels to determine the energy release profile $\dot{Q}$. The new profiles for $\dot{m}$ and $\dot{Q}$ are then used as driving functions for the wave dynamics submodel, and are updated at the end of the next cycle. The cycle end occurs when the combustion chamber pressure once again passes through atmospheric pressure as it is decreasing. The dynamic mode of the model is run for 100 cycles, which has been shown to be more than sufficient time to allow the solution to reach a repeatable pattern, if stable pulsations will occur.[1]

[1] To aid convergence of the pulsations, the forcing functions $\dot{m}$ and $\dot{Q}$ are only changed every other cycle, although the frequency is continuously updated, and the energy release profile $\dot{Q}$ is determined from an average of the old and the new values, weighted 85% on the old value. This produces a more continuous evolution in the dynamic system, and inhibits large cycle-to-cycle variations that may otherwise occur.

One-Dimensional Wave Submodel

A typical Helmholtz-type pulse combustor system has a large length-to-diameter ratio, allowing the wave dynamics to be modeled by an unsteady, one-dimensional method capable of resolving nonlinear wave formation. The finite-difference algorithm that simulates the wave dynamics in the Helmholtz-type pulse combustor uses MacCormack's method to integrate the unsteady, one-dimensional equations of continuity, momentum, and energy [12, 16]. The perfect gas equation of state is also used. To simulate the actual system dimensions these equations are written for variable-area geometry. They are

Continuity:

$$\frac{\partial(\rho A)}{\partial t} = -\frac{\partial}{\partial x}(\rho u A). \tag{1}$$

Momentum:

$$\frac{\partial(\rho u A)}{\partial t} = -\frac{\partial}{\partial x}(\rho u^2 A + PA) + P\frac{dA}{dx} - \rho A \frac{4f}{D}\frac{u^2}{2}\frac{u}{|u|}. \tag{2}$$

Energy:

$$\frac{\partial[\rho A(c_v T + u^2/2)]}{\partial t} = -\frac{\partial}{\partial x}[u(\rho A(c_v T + u^2/2) + PA)] + \dot{Q} - 4Dh(T - T_{\text{air}}). \tag{3}$$

Equation of state:

$$P = \rho R T. \tag{4}$$

Here, P, ρ, and T are, respectively, the local pressure, density, and temperature of the gas, c_v is the specific heat at constant volume, and u is the fluid velocity. D and A are the diameter and cross-sectional area of the combustor, and t and x are time and axial distance. Barr and Dwyer [16] present details of the numerical technique used to solve Eqs. 1–4, including the finite-difference equations.

The frictional losses in the momentum equation are estimated by assuming a constant duct friction factor, f, which was 0.04 in these simulations. This value is based on results in the paper by Dec et al. [18]. In that work, the cycle-resolved wall shear stress of the oscillating flow in a pulse combustor was compared with the shear stress obtained from quasi-steady pipe flow analysis using the mean Reynolds number to estimate the friction coefficient. They concluded that although the cycle-resolved shear stress was out of phase with the mean flow field, when averaged over the entire cycle, the steady flow analysis approximated the net momentum loss.

The heat transfer was measured directly in the tail pipe [19], providing the values for h_{tp} used in this work. The measured gas temperature at the inlet to the tail pipe was used to select the heat transfer coefficient in the combustion chamber h_{cc}. In the transition section the heat transfer coefficient was assumed to vary linearly between h_{cc} and h_{tp}.

The valving submodel, described in the next section, uses the numerically predicted combustion chamber pressure to determine the flow rate $\dot{m}$ through the flapper valve. This flow rate is introduced through the boundary conditions presented in Table 1. The time-dependent addition of

TABLE 1

Boundary Conditions

Combustion-Chamber Entrance		Tail-Pipe Exit
During Injection	Valve Closed	Entire Cycle:
$\frac{\partial P}{\partial x}=0$	$\frac{\partial P}{\partial x}=0$	$P=P_{\text{atm}}$
$T=T_R$	$\frac{\partial T}{\partial x}=0$	$\frac{\partial \rho}{\partial x}=0$
$u=u(t)=\frac{\dot{m}(t)}{\rho A}$	$u=0$	$\frac{\partial u}{\partial x}=0$

energy from combustion, $\dot{Q}$, is included in the energy equation. The cyclic variation of $\dot{Q}$ is determined in the fluid mixing and chemical kinetics submodels, which are described in subsequent sections. The energy release is assumed to occur in the first half of the combustion chamber. This assumption is consistent with experimental observations reported in Ref. 20. For numerical stability, it is further assumed that the energy release has a linear spatial variation, with most of the energy released at the combustion chamber inlet and decreasing to zero at the midpoint of the combustion chamber.

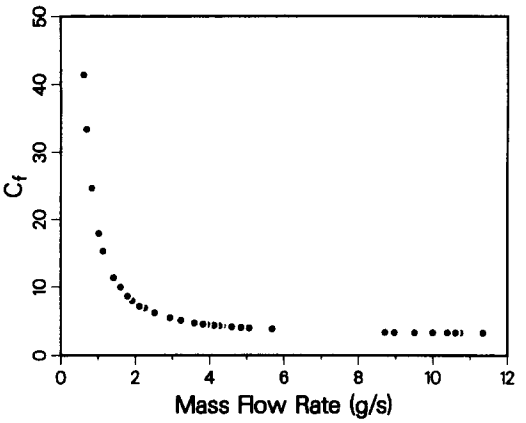

Fig. 3. Experimentally determined variation of the valve friction coefficient with Reynolds number through the valve.

Injection Submodel

The modeled valving system is a flapper valve, which is a pressure-actuated check valve. The time-varying reactant mass flow rate $\dot{m}$ is calculated from the time-varying pressure drop across the valving system. The upstream pressure is assumed to be atmospheric, while the downstream pressure is determined from the calculated results of the wave dynamic submodel described above. The time-varying mass flow rates of the reactants are calculated by assuming quasi-steady friction losses, and one-dimensional and constant density flow. With these assumptions, the equation for conservation of momentum across the valve is

$$\rho \frac{\partial u}{\partial t} = -\frac{\Delta P}{\Delta L} - \frac{\rho C_f u}{2\,\Delta L} |u|, \tag{5}$$

where ρ and u are the gas density and the mass-averaged velocity, C_f is the friction coefficient as a function of mass flow rate, ΔL is the streamwise distance over which C_f is defined, and ΔP is the pressure difference over ΔL. Invoking the quasi-steady assumption, C_f is calculated from steady-state measurements of the pressure drop across the valve being modeled over a range of flow rates, and is defined as

$$C_f = CC_f' = C\left(2\rho A_c^2 \frac{\Delta P}{\dot{m}^2}\right), \tag{6}$$

where C is a calibration coefficient. The measured variation of C_f with the mass flow rate is shown in Fig. 3. (See Ref. 21 for a complete description of the experimental facility.)

Casting Eq. 5 in terms of a mass flow rate and discretizing the equation in time and space yields

$$\dot{m}_{i+1} = \dot{m}_i - \frac{\Delta t\, C_{f_i}}{2\,\Delta L} \frac{\dot{m}_i}{\rho A_c} |\dot{m}_i| - \frac{\Delta t\, \Delta P_i\, A_c}{\Delta L}, \tag{7}$$

where $\dot{m}_i$ is the average mass flow rate at the i^{th} time step, and A_c is the cross-sectional area of the inlet.

Equation 7 is an explicit relationship for the time-varying mass flow rate. A zero mass flow rate is used to start the calculation; the mass flux at each time increment is calculated until an entire cycle is completed. The value of the calculated mass flow rate at the end of the cycle is then used for the start of a new iteration. The iterations continue until a periodic solution is achieved. The action of the flapper valve is modeled by setting the mass flow rate to zero when the calculated value is negative.

The most severe assumption in this analysis is the use of the quasi-steady friction coefficient to determine the transient flow through the valve. In the experimental system, sonic nozzles are used to control the mean flow rate. In both the experiment and the model, mass conservation is used to determine the calibration coefficient (C in Eq. 6), which corrects C_f' for unsteady effects. This

calibration coefficient is a function of mean mass flow rate and frequency of operation.

Figure 4 shows the comparison of the time-varying flow rate determined using Eq. 7 with experimental measurements of mass flow rates in an actual valve [22]. Simulations have shown that the predicted time-varying flow through the valve is not sensitive to the variation of C_f with the instantaneous Reynolds number. Virtually no difference can be detected between the $\dot{m}$ profile predicted using the C_f relation shown in Fig. 3 and that obtained with C_f held constant at the value for large flow rates taken from Fig. 3, because the flow through the valve is dominated by flow inertia and not by viscous forces.

Fluid Dynamic Mixing Submodel

The mixing of the cold reactants with the hot products in combustion chamber is a complex process. The simplified submodel used here captures the experimentally observed behavior, as is demonstrated in this article. In this submodel, the mixing is simplified by treating the injection as a single unconfined jet. The time-varying mass flow into the combustion chamber is used to determine the rate at which the cold reactants mix with the hot products. The reactants must be heated by the hot gases to a temperature T_{mix} before significant reaction can occur. This temperature, and the time scale associated with the chemistry, are specified by the chemical kinetics submodel described in the next section. In this submodel, the rate at which the cold reactants reach the temperature T_{mix} is based on transient jet analysis. The mixing rate of reactants into the combustion chamber is scaled by a single, unconfined transient jet. Although the confining geometry, the combustion process, and the oscillatory flow field make the pulse combustor's injection process much more complex than that of a single transient jet, it will be shown that this approach produces good results. By determining the single adjustable constant in the mixing model, C_{mixing}, for one set of experimental data, good agreement is obtained for changes to parameters that affect the rate of mixing, such as mean flow rate (described in the Appendix) or jet radius (described in Ref. 23).

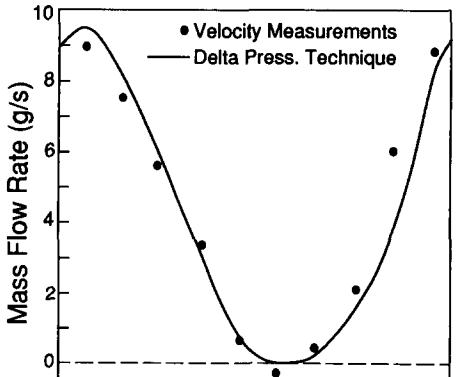

Fig. 4. Comparison of the flow rate predicted by Eq. 7 using the experimentally measured pressure difference across the valve with the flow rate determined by laser doppler velocimetry (LDV).

By assuming that the chemical delay time is much less than the fluid dynamic and natural acoustic resonance times, Bramlette [24] used the rate of fluid dynamic mixing to calculate the rate of energy release in a pulse combustor. The mixing model in that study is an extension of the model of Rife and Heywood [25]. The fluid dynamic mixing model presented in Ref. 24 includes the effects caused by mass flow rate, jet radius, combustion product temperature, and T_{mix}.

The mixing model used in this work includes an improvement to the mixing model described in Ref. 24. Although the energy release profiles predicted with the original model show good agreement with experimentally measured profiles when comparing the onset of combustion, the time-varying profiles do not show the same shapes. This discrepancy is caused by an assumption in the original model. In that work, the temporally varying injection velocity is approximated by an "equivalent" constant velocity jet (impulsively started and stopped). The magnitude and duration of this jet is determined by equating the mass and momentum fluxes of this "equivalent" jet to those of the temporally varying jet. In the modified mixing model here, the assumed constant velocity jet has been replaced with a

time-varying velocity in the mixing rate expression (Eq. A-15 of Ref. 24). This is the time-varying velocity predicted by the injection model described above. The resulting shape of the predicted energy release profile is close to that observed experimentally, as will be shown in the Results section. The improved model retains the response to system parameters, such as temperatures and injection geometries, that were displayed in the original model.

The mixing model has a single adjustable constant, C_{mixing}, that is determined by matching model predictions with a single set of experimental data. With this constant fixed, the model can be used to predict trends when other process variables or geometrical characteristics are changed [24]. The coupling of this mixing model in the pulse combustor simulation produces a dynamic algorithm in that the mixing model is both driven by, and acts to drive, the wave dynamics.

Chemical Kinetics Submodel

The fluid dynamic mixing model predicts the rate at which the injected reactants mix with the hot products to a temperature T_{mix} at which significant reaction occurs. This temperature depends on the chemical composition of the reactants. Once the reactants reach T_{mix}, chemical reaction takes place. The chemical kinetics submodel assumes the reaction takes place in a well-stirred reactor [26]. Although the reaction process is much more complex in a pulse combustor than in a well-stirred reactor, this simplification is necessary to make the problem tractable. Results presented in the Appendix verify that this submodel captures the dominant mechanism produced by the chemical kinetics.

To determine the time delay before reaction, the submodel assumes that a mixture of methane and air, initially at 300 K and therefore virtually unreactive, is steadily diluted and heated by mixing with the hot products of the complete reaction. The products are assumed to have a temperature equal to the adiabatic flame temperature of the mixture. The present chemical kinetics calculations were carried out using the HCT code [27], which solves the coupled equations of conservation of mass, momentum, energy, and chemical species. The detailed reaction mechanisms for the oxidation of mixtures of methane and ethane are listed in Refs. 17, 28, and 29.

The rate of mixing used in the kinetics submodel was chosen to be as close as possible to that observed in the experiments and described by the jet mixing submodel discussed in the previous section. As the reactants are heated by this mixing process, oxidation reactions proceed at rates that are significant when related to the rate of mixing, beginning at approximately 1200 K. The rate of methane combustion continues to increase as the dilution with hot products continues. The result of this procedure is the ignition of the methane–air mixture, superimposed upon a steady heating and dilution caused by the mixing with the hot combustion products.

This type of modeling calculation was carried out for methane–air mixtures with fuel equivalence ratios from $\phi = 0.4$ to 1.5. For each value of the equivalence ratio, the influence of dilution by addition of excess N_2 was examined, beginning with normal fuel–air mixtures and ranging up to 40% excess N_2 by weight. In every case, the nature of the ignition was found to depend on the value of the adiabatic flame temperature, T_{flame}. Conditions with ignition are summarized in Table 2. When T_{flame} falls below about 1450 K, the cold reactant mixture never reaches a temperature that is high enough for ignition to occur. In such cases, the reactants become thoroughly diluted by reaction products before any ignition can take place.

At the very lowest values of ϕ, even fuel–air mixtures undiluted by excess N_2 will not ignite under the present conditions. For values of the equivalence ratio between 0.5 and 0.6, and for values above $\phi = 1.3$, mixtures with as much as 30% excess N_2 were capable of ignition, although addition of 40% excess N_2 prevented ignition, as listed in Table 2. Between the limits $0.7 < \phi < 1.3$, all fuel–air mixtures ignited for conditions with up to 40% excess N_2.

For each mixture, it was found that there is a critical value of the temperature at which the reaction time t_{react} becomes short compared with

TABLE 2

Effect of Nitrogen Dilution and Equivalence Ratio on Various Properties

Adiabatic Flame Temperature T_{flame} (K)

ϕ	Y_{N_2} = 0	0.1	0.2	0.3	0.4
0.6	1665	1560	1475	1400	[a]
0.8	2000	1880	1770	1680	1600
1.0	2245	2120	2020	1920	1835
1.2	2130	2010	1900	1800	1715
1.4	1980	1860	1760	1675	1600

Temperature for Significant Reaction T_{mix} (K)

ϕ	Y_{N_2} = 0	0.1	0.2	0.3	0.4
0.6	1480	1450	1410	1360	[a]
0.8	1585	1580	1560	1530	1510
1.0	1645	1645	1640	1635	1620
1.2	1660	1640	1620	1600	1580
1.4	1640	1620	1580	1540	1500

Ignition Delay Time t_{react} (ms)

ϕ	Y_{N_2} = 0	0.1	0.2	0.3	0.4
0.6	0.55	0.8	1.25	2.4	[a]
0.8	0.35	0.45	0.55	0.95	1.1
1.0	0.35	0.5	0.7	1.0	1.7
1.2	0.45	0.7	1.1	2.0	3.6
1.4	0.75	1.3	2.4	4.0	6.7

[a] Mixture did not burn.

the mixing time and all of the remaining fuel–air mixture is consumed. This critical temperature is a weak function of the equivalence ratio and degree of dilution, having values in the range of 1350–1650 K for all of the mixtures considered. In mixtures with little or no excess N_2 dilution and mixtures close to stoichiometric, both with relatively high values of T_{flame}, the reactants reach this ignition temperature more quickly than mixtures with smaller values of T_{flame}, since less mixing is required to achieve the ignition temperature. Furthermore, since less mixing is needed to achieve the ignition temperature, the amount of fuel consumed in the ignition is greater and the heat release is therefore greater than for mixtures with lower values of T_{flame}.

These computations permit a relationship to be established among the fuel–air equivalence ratio, the rate of mixing, and the rapid ignition of the reactant mixture which included the details of the chemical kinetics of ignition under the conditions within the pulse combustor. These results are then used as parameters to convert the results from the mixing model to an energy release profile that is used to drive the wave dynamics of the pulse combustor.

Model Limitations

Many simplifying assumptions have been made in this model of a pulse combustor. Results presented in the next section and in the Appendix show that the combination of these relatively simple submodels produces a model that closely reproduces behavior observed in experiments.

Possible improvements to the model include using a multidimensional finite-difference technique to simulate the mixing and reaction processes that occur in the combustion chamber. The current mixing model is restricted to injection flow characteristics that scale with free jets. Many pulse combustors use complex injection geometries, with the fuel and air injected at different locations in the combustion chamber and at different times during the cycle. An improved submodel could combine a sophisticated turbulence model, species transport algorithms, and detailed chemical kinetics modeling, including extinction by fluid dynamic stretch, all of which would require a fine numerical grid to resolve the small length scales of importance. In the wave dynamics submodel, the wall friction and heat transfer are treated in a quasi-steady manner. Experimental results have indicated that this assumption may not be valid for flows with strong oscillations [18, 19]. To remove the empiricism in the friction and heat transfer terms, the viscous and thermal boundary layers in the entire system, especially in the tail pipe, should also be included in the model.

The combination of these features in an oscillating flow field challenges current modeling and computational capabilities. Although the assump-

tions in the model simplifying dominant processes, results presented in this article show that the model is still very powerful.

RESULTS: VERIFICATION OF THE MODEL

This section presents a direct comparison of results from the model with experimentally obtained results [30]. As discussed below, this is the base calculation to which the adjustable constants were tuned. It is also the base conditions for the parametric study. The Appendix contains additional comparisons with experimental results over a range of nitrogen dilutions, mean flow rates, and a longer tail pipe configuration. The comparisons show that the model is capable of reproducing the experimentally observed behavior of a pulse combustor over a wide range of operating conditions without varying these adjustable constants. It is able to identify experimental operating conditions that cannot support a pulsing mode.

The dimensions of the system used in these calculations were chosen to match those of the experimental Helmholtz-type pulse combustor under study at Sandia [12–14, 16–24, 30]. This combustor consists of a 100-mm-long combustion chamber 75 mm in diameter, and typically a 880-mm-long tail pipe of 30 mm diameter, joined by a 130-mm-long transition section with a linearly varying side width. The volume of the mixing chamber used in the experiment is accounted for by adding 16 mm to the combustion chamber length in the model. A uniform grid consisting of 112 cells is used in most of the simulations. For geometries with longer tail pipes discussed in the Appendix, additional cells are used to maintain comparable resolution. The experimental pulse combustor has a square cross section to allow optical access throughout the entire combustor, and this characteristic is retained in the model through the definitions of A and D.

For this base computation, the combustible gas is a mixture of methane–air at an equivalence ratio ϕ of 1.02 that is diluted with 12% nitrogen by mass, that is, $Y_{N_2} = 0.12$. The mean flow rate is $\bar{\dot{m}} = 4.0$ g/s, which combines with the reactant mixture to fix the cycle-averaged energy release rate $\bar{\dot{Q}}$. To reproduce the experimental operating conditions, both the heat transfer coefficient in the tail pipe h_{tp} and the surrounding air temperature T_{air} used in the model have been obtained from the experiment [30]. The parameters used in the base calculation are summarized in Table 3.

TABLE 3

Parameters Used in Base Calculation

Parameter	Value
Equivalence ratio	$\phi = 1.02$
Dilution	$Y_{N_2} = 0.12$
Tail pipe length	$L_{tp} = 0.88$ m
Mean mass flow rate	$\bar{\dot{m}} = 4.0$ g/s
Friction coefficient	$f = 0.04$
Heat transfer coefficients	$h_{tp} = 51.8$, $h_{cc} = 30$ W/m^2/K
External temperature	$T_{air} = 384$ K
Mixing model parameter	$C_{mixing} = 0.17$

The base calculation was used to tune the two adjustable constants in the model: the heat transfer coefficient in the combustion chamber (h_{cc}), and a constant C_{mixing} used in the mixing model. These values were then used in all other simulations presented in this article, unless noted otherwise. The numerical algorithm described below was repeated for different values of these constants until the results agreed with the experimental results. From these simulations the value of $h_{cc} = 30$ W/m^2/K was selected to match the experimentally measured cycle-averaged gas temperature at the tail pipe inlet. The experimentally observed operating frequency was used to tune C_{mixing}. The value of $C_{mixing} = 0.17$ produces good agreement.

Although the pressure wave, the mass injection profile $\dot{m}$ and the energy release profile $\dot{Q}$ are highly coupled, only a few cycles are required before stable periodic oscillations start to develop, as can be seen in Fig. 5 which shows the operating frequency for the first 50 cycles after the model has been switched to the dynamic mode. After 100 cycles, the operating frequency is 82.0 Hz. The convergence of the solution is indicated by the variation of the operating fre-

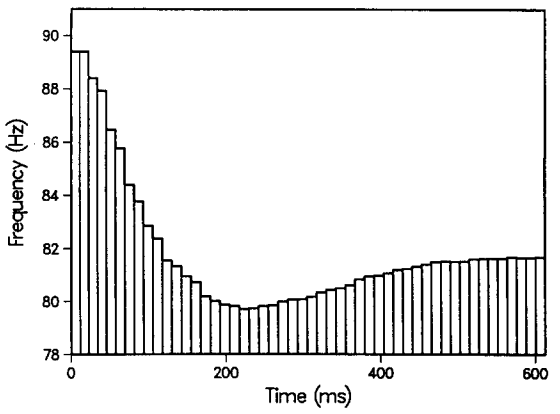

Fig. 5. Evolution of the frequency from startup of the dynamic simulation showing development of a repeatable wave pattern.

quency, which changed by less than 0.1% during the last 20 cycles.

The simulation produces a pressure signal in the combustion chamber that is in good agreement with experiments, with a pressure rms (root mean square about the mean value) of P_{rms} = 7.45 kPa, which differs by less than 2% from the experimentally measured value of 7.32 kPa. The rms pressure is in surprisingly good agreement considering that no parameter was adjusted to match the experimentally measured value. The time-varying combustion chamber pressure is produced by the wave dynamics in the entire system. The good agreement of the rms pressures supports the findings of Dec et al. [18] that the Reynolds number of the mean flow can be used to estimate the friction coefficient for quasi-steady friction loss analysis, removing the correct amount of momentum from the flow when averaged over a cycle (see Eq. 2).

The injection and energy release profiles, $\dot{m}$ and $\dot{Q}$, from this dynamic simulation are compared with the experimentally measured profiles in Fig. 6. As shown in Fig. 6, the injection profile obtained from the dynamic simulation is similar to that measured in the experiment. The differences in $\dot{m}$ profiles may be caused by the simplifications in the model. It is assumed in the model that the tube connecting the flapper valve to the combustion chamber has a minimal affect. However, this line does change the pressure signal that reaches the valve, which could explain the differences between the cycle times at which the maximum injection occurs. Figure 6 also shows that the energy release profile $\dot{Q}$ from the model resembles the experimentally obtained profile, with maxima and minima that occur at similar normalized cycle times. As was previously described, the model uses the injection profile to determine the energy release profile. Although the value of the constant C_{mixing} in the mixing

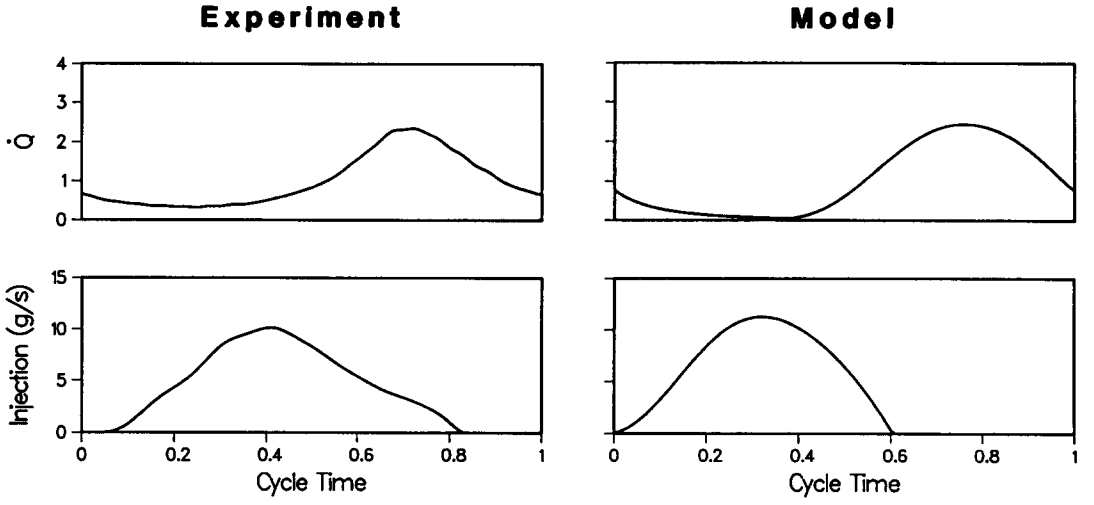

Fig. 6. Time-varying mass injection and normalized energy release profiles from both the experiment and the simulation. The time scales have been normalized by the operating frequency.

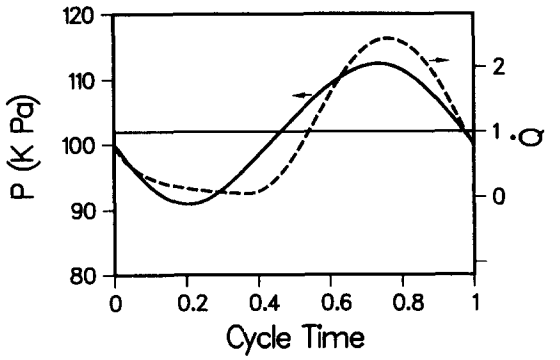

Fig. 7. Phase relation between the combustion chamber pressure (solid line) and normalized $\dot{Q}$ profile (dashed line) versus cycle time. The horizontal line corresponds with both the mean pressure and the mean normalized energy release.

model was selected to match operating frequencies, this value is also correcting for the differences in the injection profiles.

The model predicts that the resulting energy release profile is sufficient to support stable pressure oscillations. Based on Rayleigh's criterion, this indicates that enough energy is being released during the high-pressure portion of the cycle to replace the energy in the oscillations that is lost to mechanisms including wall friction. Figure 7 shows the relative phase of the pressure and energy release profiles. The horizontal line marks the mean values of both curves. Figure 7 shows that although the two curves are enough in phase to maintain oscillations, during several portions of the cycle the energy release is acting to retard the oscillations. Rayleigh's criterion indicates that stronger pulsations could be obtained by "tuning" the system to increase the phase relation. In the next section, single parameters are varied to effect this tuning. The selected parameters directly affect just one of the characteristic times ($\tau_{acoustic}$, τ_{mixing}, and $\tau_{kinetic}$). This allows for better control, clearly demonstrating the cause–effect relationship.

RESULTS: DEMONSTRATION OF THE IMPORTANCE OF CHARACTERISTIC TIMES

The effect of the characteristic time scales has been investigated by using the numerical model to change each time scale while minimizing the impact on the other operating conditions. These time scales are associated with the acoustics, the fluid mixing, and the chemical kinetics of the pulse combustor. All other parameters are held at the values used in the base calculation (listed in Table 3). Although experimental investigations of this type [13, 14] have demonstrated the importance of the time scales, the strong coupling between all of the dominant phenomena in the pulse combustor makes it hard to firmly establish the cause–effect relationship. The numerical model provides more control over the processes.

Effect of the Acoustic Time Scale $\tau_{acoustic}$

The acoustic time scale $\tau_{acoustic}$ is determined by the time required for a pressure wave to travel the length of the pulse combustor. This time scale can be increased by lengthening the tail pipe, as is described in the Appendix. Because the sound speed scales with the square root of the temperature field, the acoustic time scale can also be changed by varying the temperature distribution in the tail pipe. Figure 8 shows the variation of frequency and rms pressure with h_{tp}, plotted in normalized units using the base condition value from Table 3. As expected, as the heat transfer coefficient is increased the frequency drops because the mean temperature also drops. The model predicts that the combustor will not pulse for heat transfer coefficients that are less than 60% of the base value. For h_{tp} set to twice the value from the base condition, the operating frequency is 75.7 Hz, as compared with 82.0 Hz for the base condition. This indicates that the operating frequency is not very sensitive to the value of the heat transfer coefficient. For large values of the heat transfer coefficient, the frequency is essentially constant, indicating that the gas temperature in the tail pipe is in equilibrium with the surrounding environment.

Figure 8 also shows that the rms pressure increases as the temperature drops, indicating that the phase relation between the pressure wave and the energy release is becoming more favorable. This is consistent with the results from the base calculation. Figure 7 showed that the pressure wave in the base calculation was preceding the energy release profile, and Rayleigh's criterion

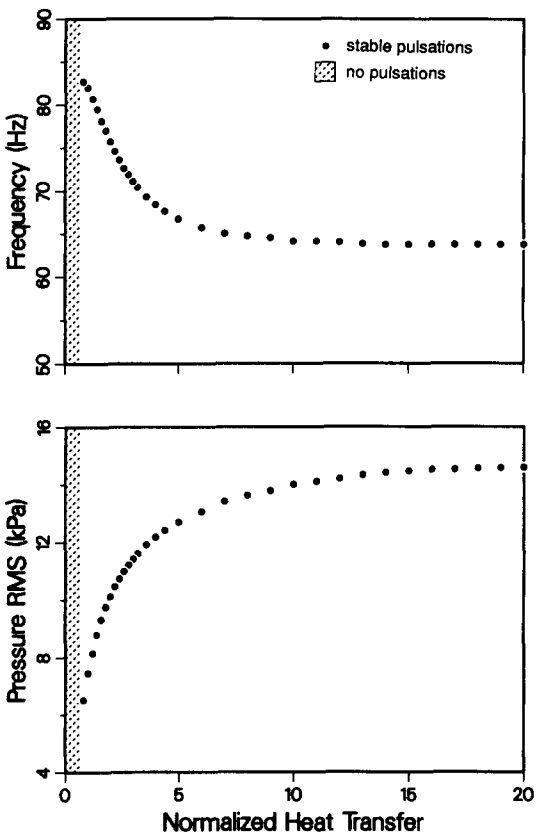

Fig. 8. Sensitivity of the pulsations to the characteristic time of the acoustics. Values of the heat transfer coefficient have been normalized by h_{tp} from the base condition (listed in Table 3).

indicated that stronger pulsations could be obtained by increasing the acoustic time scale. The results presented in Fig. 8 show that slowing down the mean sound speed produces significantly larger pressures. The maximum rms pressure is almost twice that from the base condition.

Effect of the Fluid Mixing Time Scale τ_{mixing}

Another method of improving the phase relation between the pressure wave and the energy release profile from the base condition is to speed up the energy release, while not changing the sound speed. This can be accomplished by changing the rate at which the cold reactants mix with the hot products [23]. Results in the Appendix show that the mixing can be improved by increasing the mean reactant flow rate without changing the injection geometry. These simulations used the value for the adjustable constant in the mixing model, C_{mixing}, that was selected from the base calculation to represent the fluid mixing from the experiment. The mixing submodel reproduced the improved mixing that occurs at the larger mean flow rates, and the model correctly captured the resulting changes in performance of the pulse combustor, as discussed in the Appendix.

For a fixed mean mass flow rate, the mixing can be improved by changing the injection system, either by decreasing the diameter of the inlet or by changing some other feature of the injection geometry. To speed up the rate of the mixing, the constant C_{mixing} is decreased. As Fig. 9 shows, as the mixing rate is increased, the combustor

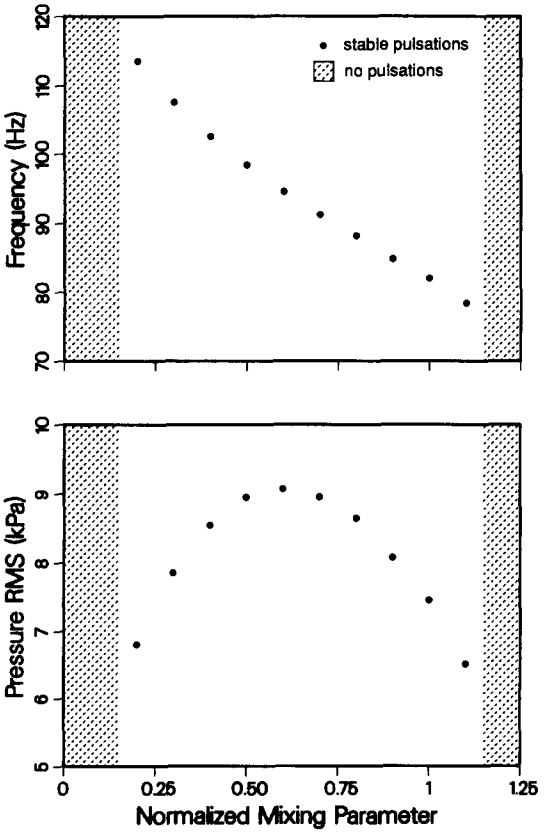

Fig. 9. Sensitivity of the pulsations to the characteristic time for mixing. Plotted values of the mixing constant C_{mixing} have been normalized by the value from the base condition (listed in Table 3).

operates at higher frequencies, even though the sound speed has not been changed. The earlier energy release is pushing the pressure wave earlier in the cycle. This shift in the energy release profile also increases the rms pressure, as was experimentally determined from Rayleigh's criterion [13, 14]. The rms pressure reaches a maximum, and as the mixing rate is further increased the pressure decreases, indicating that there is an optimal mixing rate for the system.

Effect of the Chemical Kinetics Time Scale $\tau_{kinetic}$

In addition to changing the fluid mixing to shift the energy release profile, chemical kinetics can also be used. Dilution of the reactants with nitrogen changes the chemical kinetics. A comparison of results from the model with experimental measurements obtained at different reactant dilutions is described in the Appendix. In those simulations, other parameters, such as the heat transfer coefficients, had to be adjusted to each experimental operating condition. In the simulations presented here, the effect of chemical kinetics is isolated by holding all other parameters constant.

In our chemical kinetics submodel, the combustible mixtures are characterized by three parameters: the adiabatic flame temperature T_{flame}, the temperature for significant reaction T_{mix}, and the chemical delay time t_{react}. Because the value of T_{flame} affects the mean temperature of the gas, it affects the acoustics. The value of T_{mix} determines how much mixing of the cold reactants with the hot products must occur before reaction can take place. The higher the value, the longer the mixing will take. The chemical delay time t_{react} is effectively added to the total delay time between injection and burning. Because the value of T_{flame} affects the mean temperature of the gas, it affects the acoustics.

Several simulations were performed using two different mixtures, both of which have the same adiabatic flame temperature as that from the base condition, but these gases have different combustion delay times and different reaction temperatures T_{mix}, as listed in Table 4. The equivalence ratios of these mixtures are $\phi = 0.6$ and 1.225, with no additional nitrogen. The resulting operating conditions were affected by the small differences in the mixtures, as listed in the table. Although differences in the chemical delay time should directly change the cycle time, the frequencies are dominated by the changes to T_{mix}. This indicates that for this set of gases, fluid mixing is still controlling the pulse combustor operation.

Another set of simulations was performed to isolate the affect of the chemical delay time. These results are summarized at the bottom of Table 4. In this set, the only parameter that was changed from the base condition is t_{react}. The cycle times increase almost exactly in agreement with the changes to t_{react}, as was proposed by

TABLE 4

Effect of Chemical Kinetics

ϕ	Y_{N_2}	T_{flame} (K)	T_{mix} (K)	t_{react} (ms)	Freq (Hz)	P_{RMS} (kPa)
0.86	0	2102.0	1607.8	0.336	87.0	8.29
1.02*	0.12	2102.9	1646.2	0.551	82.0	7.45
1.225	0	2103.4	1659.2	0.474	80.7	7.16
†		2102.9	1646.2	0.	85.5	8.08
1.02*	0.12	2102.9	1646.2	0.551	82.0	7.45
†		2102.9	1646.2	1.102	78.2	6.61

* Base Condition.

† Fuel is "computer gas".

Keller et al. [13]. Because the shorter chemical delay times cause the energy release profile to occur earlier in the cycle, a larger rms pressure relative to that from the base calculation is produced by the mixture with the shorter delay time, in agreement with Rayleigh's criterion [13, 14].

Combined Effect of the Time Scales $\tau_{acoustic}$, τ_{mixing}, and $\tau_{kinetic}$

The results presented so far indicate that the performance of a pulse combustor can be optimized by making changes to the operating conditions. Most of these changes affect all of the characteristic times. For example, changing the combustible gas mixture changes all parameters associated with the kinetics, including the adiabatic flame temperature. Because the entrainment rate of a jet into a quiescent fluid depends on the density ratio, the addition of nitrogen affects the fluid mixing rate. Also, because the mean temperature of the gas changes with T_{flame}, the sound speed also changes. The heat transfer coefficient is affected by changes to the pulsation strength and frequency [30], although the results presented in Fig. 8 show that the frequency is not strongly controlled by the heat transfer.

Figure 10 shows the response of a pulse combustor to changes in the combustible mixture. In this case, the tail pipe length is twice that from the base condition: $l_{tp} = 1.76$ m. The mean mass flow was fixed at 4.5 g/s and the equivalence ratio was $\phi = 1.02$, but the nitrogen dilution was increased from no additional nitrogen to 40% by mass. Figure 10 shows that as the fuel flow rate is decreased (replaced by nitrogen) the frequency drops. However, the pressure oscillations can be increased by replacing some of the combustible mixture with nitrogen, thus reducing the amount of fuel relative to the case with no dilution. This is an example of using nitrogen to "tune" the system. Further addition of nitrogen causes the pulsations to decrease in magnitude, indicating that the parameters are no longer optimal. Similar results obtained in an experimental pulse combustor showed that dilution by nitrogen was sufficient to produce a tuned combustor [13]. Use of the characteristic fluid mixing time to change the system performance has been demonstrated in a commercial pulse combustor [23].

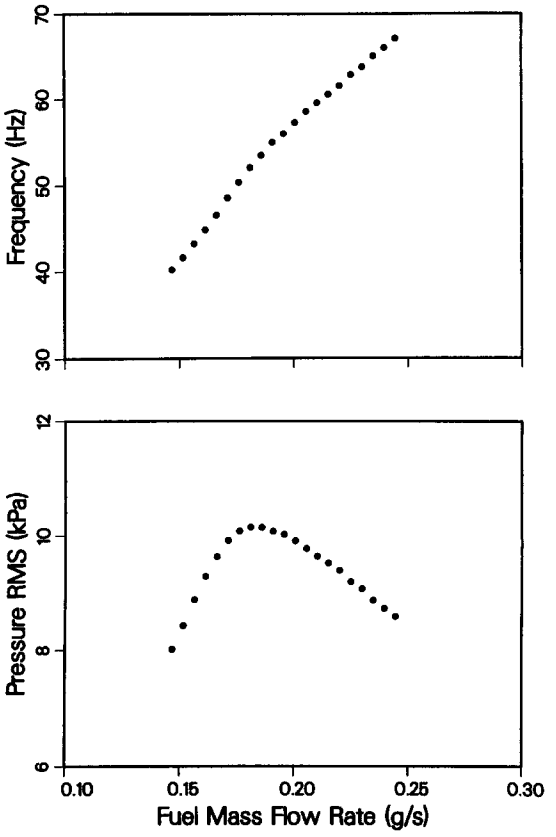

Fig. 10. Sensitivity of the pulsations to variations in the fuel flow rate. Total mass flow and equivalence ratio were constant, the amount of nitrogen was increased from zero (far right) to 40% (far left). The peak in the rms pressure indicates optimal conditions for pulsations.

CONCLUSIONS

We have combined submodels for the cycle-resolved injection and energy release profiles occurring in a pulse combustor to track the resulting wave motion. The combination of these submodels produces a pulse combustor model that couples the major processes, making it dynamic in nature because the performance of each of these submodels depends on the performance of the others. The wave pattern is followed in time by integrating the unsteady, one-dimensional, variable-area equations of continuity, momentum and

energy, including losses due to friction and heat transfer. The injection model assumes the reactant flow rate is driven by the pressure drop across a flapper valve. The rate of combustion of the cold reactants is described by a combination of the rate of fluid dynamic mixing and the rate of chemical reaction. The resulting model is in good agreement with experimental observations, reproducing the trends observed in the experimental data for changes to several operating parameters.

Results from the model show that the operating frequency and pulsation magnitude can be varied by changing the phase relation between the energy release and the pressure oscillations, consistent with the work by Rayleigh. The acoustics can be varied by changing the temperature field. Changes to the injection geometry or the chemical kinetics affects the time delay between injection and reaction of the fresh reactants. The parametric study shows that the operating frequency is not very sensitive to changes in the heat transfer coefficient even though this affects the sound speed. However, because the sound speed affects the phase relation between the combustion chamber pressure and the energy release, the magnitude of the pulsations can be more sensitive to the heat transfer (a factor of 2 increase in h_{tp} decreases the frequency by 8% and increases the rms pressure by 36%). Consistent with experimental results, fluid mixing of the cold reactants with the hot products provides the most control of the time-varying energy release profile [14, 23]. Adjustments to the mixing can be accomplished by changing the injection geometry (changing the location and size of the inlet tubes). Results from the model also show that chemical kinetics can be used to make fine adjustments to the phase relation between the energy release and the combustion chamber pressure.

Because independent control of parameters that determine different time scales is possible with the numerical model, the concept of characteristic times for pulse combustor performance has been strengthened by the results presented here.

We would like to thank Eldon Porter for his continued assistance in the laboratory. This work was performed at the Combustion Research Facility, Sandia National Laboratories supported by the U.S. Department of Energy, Energy Conservation and Utilization Technologies Program, and at the Lawrence Livermore National Laboratory supported by the U.S. Department of Energy and the Gas Research Institute.

REFERENCES

1. Rayleigh, J. W. S., *Nature* 18:319 (1878); also *The Theory of Sound*, Dover, New York, 1945, vol. 2, p. 226.
2. Zinn, B. T., ASME Paper 84-WA/NCA-19, ASME Winter Annual Meeting, New Orleans, LA, December 1984.
3. Putnam, A. A., in *Proceedings of the First International Symposium of Pulsating Combustion*, (D. J. Brown, Ed.), 1-1 to 1-45, Department of Chemical Engineering and Fuel Technology, University of Sheffield, Sheffield, England, September 1971.
4. Putnam, A. A., ASME Paper 84-WA/NCA-20, ASME Winter Annual Meeting, New Orleans, LA, December 1984.
5. Vishwanath, P. S., GRI-85/0280, Gas Research Institute, Chicago, IL, 1985.
6. Bhaduri, D., Boxi, C. B., Gill, B. S., and Mukhopadhyay, N., *Ind. J. Technol.* 6:245 (1968).
7. Craigen, J. G., Ph.D. thesis. The University of Durham, United Kingdom, 1975.
8. Clarke, P. H., and Craigen, J. G., in *Proceedings of the Sixth Thermodynamic and Fluid Mechanics Convention*, Durham, United Kingdom, 1976, p. 221.
9. Coulman, G. A., Vishwanath, P., Alhaddad, A., and Bartam, P. N., in Proceedings of the Symposium on Pulse Combustion Applications, 6-1 to 6-15, Atlanta, GA, March 1982, available from NTIS, Paper No. 6.
10. Ponizy, B., and Wojcicki, S., Presented at the 1982 Fall Meeting of the Western States Section of the Combustion Institute, Livermore, CA, 1982, paper no. 82-71.
11. Lee, J. J-H., Ph.D. thesis, Purdue University, Lafayette, IN, 1983.
12. Barr, P. K., Dwyer, H. A., and Bramlette, T. T., *Combust. Sci. Technol.* 58:315 (1988).
13. Keller, J. O., Dec, J. E., Westbrook, C. K., and Bramlette, T. T., *Combust. Flame* 75:33 (1989).
14. Keller, J. O., Bramlette, T. T., Dec, J. E., and Westbrook, C. K., *Combust. Flame* 79:151 (1990).
15. Tsujimoto, Y., and Machii, N., *Twenty-First Symposium (International) on Combustion*, The Combustion Institute, Pittsburgh, 1987.
16. Barr, P. K., and Dwyer, H. A., *Progress in Aeronautics and Astronautics: Numerical Approaches to Combustion Modeling*, (E. Oran and J. Boris, eds), AIAA, Washington DC (in press).
17. Keller, J. O., and Westbrook, C. K., *Twenty-First*

Symposium (International) on Combustion, The Combustion Institute, Pittsburgh, 1987.
18. Dec, J. E., Keller, J. O., and Hongo, I., Combust. Flame (in press).
19. Dec, J. E., and Keller, J. O., *Combust. Flame* 80:358 (1990).
20. Keller, J. O., and Hongo, I., *Combust. Flame* 80:219 (1990).
21. Keller, J. O., and Saito, K., *Combust. Sci. Technol.* 53:137 (1987).
22. Keller, J. O., Sandia National Laboratories Report SAND86-8775.
23. Keller, J. O., Barr, P. K., Bramlette, T. T., Evens, L., and Marchant, R., *Combust. Sci. Technol.* 66:127 (1989).
24. Bramlette, T. T., Sandia National Laboratories Report SAND87-8622, 1987.
25. Rife, J. M., and Heywood, J. B., *SAE Trans.* 83:2942 (1974).
26. Westbrook, C. K., Pitz, W. J., Thorton, M. M., and Malte, P. C., *Combust. Flame* 72:45 (1988).
27. Lund, C. M., University of California Lawrence Livermore National Laboratory Report UCRL-52504, 1978.
28. Westbrook, C. K., *Combust. Sci. Technol.* 20:5 (1979).
29. Westbrook, C. K., and Pitz, W. J., *Combust. Sci. Technol.* 37:117 (1979).
30. Dec, J. E., and Keller, J. O., *Combust. Flame* 77:359 (1989).

Received 27 March 1989; revised 30 August 1989

APPENDIX: VALIDATION OF THE MODEL

This appendix presents additional comparisons of results from the model with experimentally obtained results [30] in an operating Helmholtz-type pulse combustor. The operating conditions for these simulations are summarized in Table A1. The dimensions of the system used in these calculations are the same as those from the base case described in the article. These results show that the model can predict the experimentally observed trends for changes to the operating conditions without tuning the adjustable constants in

TABLE A1

Parameters and Results from the Verification Simulations[a]

L_{tp} (m)	$\bar{\dot{m}}$ (g/s)	Y_{N_2}	h_{tp} (W/m^2 K)	T_{air} (K)	Frequency (Hz) Exp.	Frequency (Hz) Model	P_{RMS} (k Pa) Exp.	P_{RMS} (k Pa) Model
0.88	3.6	0.08	49.0	381	80.3	82.4	7.16	7.37
0.88	3.6	0.12	48.0	378	78.4	78.7	6.53	6.53
0.88	3.6	0.20	19.9	368	—	—	—	—
0.88	3.6	0.24	17.8	368	—	—	—	—
0.88	4.0	0.08	51.7	386	85.4	85.5	7.61	8.04
0.88[b]	4.0	0.12	51.8	384	82.4	82.0	7.32	7.44
0.88	4.0	0.14	51.1	381	80.6	80.1	7.06	6.98
0.88	4.0	0.20	23.4	369	—	—	—	—
0.88	4.9	0.08	54.3	404	91.0	91.3	8.64	9.25
0.88	4.9	0.10	55.2	405	89.3	89.3	8.59	9.02
0.88	4.9	0.22	28.2	387	—	—	—	—
0.88[c]	4.9	0.22	51.8	384		—		—
1.28	4.0	0.10	40.8	396	67.9	72.5	7.90	9.10
1.28	4.0	0.14	39.7	392	66.5	69.9	7.17	8.90
1.28	4.0	0.16	39.2	388	65.8	68.6	6.64	8.74
1.28	4.0	0.18	38.2	386	65.4	67.2	6.00	8.47
1.28	4.0	0.24	17.6	374	—	—	—	—

[a] Experimental results from Ref. 30. In all simulations, $\phi = 1.02$, $h_{cc} = 30$, and $f = 0.04$. The dash (—) identifies systems that would not pulse.

[b] Base condition.

[c] Sensitivity test: h_{tp} and T_{air} are from base case.

the model. The model also shows that for certain operating conditions pulsations cannot be maintained. These conditions do not allow pulsations to occur in the experimental pulse combustor.

Effect of Nitrogen Dilution

The model reproduces the experimentally observed changes in performance when excess nitrogen is added to the mixture. Changing the dilution affects all of the characteristic times because additional nitrogen influences both the temperature T_{flame} and T_{mix}, as well as the chemical kinetics, as shown in Table 2. Other parameters in the simulation are those from the base calculation listed in Table 3, with the values of the heat transfer parameters as listed in Table A1. Because the mean mass flux is held constant at $\bar{m} = 4.0$ g/s, the additional nitrogen replaces some of the fuel-air mixture. As indicated in Table 2, when the nitrogen dilution Y_{N_2} is increased at constant equivalence ratio, the adiabatic flame temperature T_{flame} decreases and the chemical delay time t_{react} increases. Both of these effects act to decrease the operating frequency at higher nitrogen dilution, as shown in Table A1. The rms pressure in the combustion chamber also decreases for increasing nitrogen fractions, consistent with the experimental results.

Both the model and the experiment show that when the nitrogen concentration is increased to $Y_{N_2} = 0.20$, the combustor is unable to support pulsations and the combustor stops operating. This is because the additional nitrogen affects the relative phasing of the pressure wave and the energy release profile to the point where pulsations can no longer be sustained, consistent with Rayleigh's criterion. The agreement of the model with the experiment is remarkable considering that the two adjustable constants in the model have been held constant at the values determined in the base calculation.

Effect of Tail Pipe Length

Consistent with the experimental results, when the pulse combustor is operated with a longer tail pipe (increased 45% from $L_{tp} = 0.88$ m to $L_{tp} = 1.28$ m), the model predicts that the frequency decreases to account for the increase of the acoustic resonance time scale τ_{acoustic} that occurs for longer tail pipes. The model correctly predicts the trends for the addition of nitrogen, including the termination of pulsations at large nitrogen dilution, as shown in Table A1. The maximum error in the predicted frequency is 7%, but the rms pressure is overpredicted by up to 41%. These errors indicate that the physical phenomena represented by the constants h_{cc} and C_{mixing} have been affected by the change in the geometry, although the shut off of the system at $Y_{N_2} = 0.24$ in both the simulation and the experiment indicates that the dominant phenomena are still reproduced in the model. A sensitivity computation was performed to ensure that the model's prediction of the nonpulsing case was not affected by the lower heat transfer coefficients measured in the nonpulsing cases (Table A1). The simulation was repeated using the values of h_{tp} and T_{air} from the base case, and the model predicted that the system was still unable to support pulsations.

Effect of Mean Mass Flow

Larger mean flow rates produce higher rates of mixing of the cold reactants with the hot products. This increase in the mixing rate leads to a smaller value of τ_{mixing} because it takes less time for the cold gas to reach a temperature at which significant reaction can occur. Thus, for larger flow rates, there is less time between injection and combustion. The effect of this is indicated in both the numerical and experimental results presented in Table A1. As the mass flow rate is increased, the operating frequency increases because the energy release is pushed earlier in the cycle, again consistent with Rayleigh's criterion.

The rms pressure also increases with increasing flow rates. This is a consequence of Rayleigh's criterion. As described before, the operation of the flapper valve ties the injection of the reactant to the low pressure portion of the cycle. Because in this work only the mixing has been significantly changed, the higher flow rates are pushing the energy release to be in phase with the pressure wave, causing the rms pressure to increase.